Applications of Adaptive Optics for Vision Science

Yasuki Yamauchi*, Austin Roorda[†], David R. Williams*[,♯], Jason Porter*[,♯], and Antonio Guirao*[,‡]

∗ *Center for Visual Science, University of Rochester, Rochester, New York, 14627, USA*

† *College of Optometry, University of Houston, 4901 Calhoun Blvd., Houston, Texas, 77204, USA*

‡ *Laboratorio de Optica, Universidad de Murcia, Campus de Espinardo (Edificio C), 30071 Murcia, SPAIN*

♯ *The Institute of Optics, University of Rochester, Rochester, New York, 14627, USA*

1. Introduction

There are a number of applications of adaptive optics for basic research in vision science, as it is now possible to study microstructures in the living human retina which could not be done before. One of the biggest merits provided by adaptive optics is that it is non-invasive. In this chapter, we describe the applications of an adaptive optics system for vision research, not only for basic science, but also for clinical fields. First, we will briefly explain how to obtain high resolution images of the living human retina with adaptive optics.

2. Retinal Imaging in Living Human Eyes

Imaging the living human retina has been possible for 150 years since the invention of the ophthalmoscope by Helmholtz. Since that time, retinal imaging has been an invaluable tool for applications ranging from the clinical diagnosis of retinal diseases to studying the fundamentals of human vision. Helmholtz's ophthalmoscope did not use a camera, but rather used the practitioner's eye as the detector as shown in Fig. 1(a). The principle used was quite simple. The main problem with this early ophthalmoscope was that the doctor had to shine a light into the eye along the same axis that he needed to simultaneously place his own eye in order to look at the retina. Helmholtz later modified his ophthalmoscope by incorporating a beamsplitter to provide two separate paths, one that allowed light to enter the eye and illuminate the retina, and the other that allowed for the simultaneous capture of the reflected fundus image. This method non-invasively enabled Helmholtz to obtain low-resolution images of the retina since he was unable to correct for the aberrations of the eye.
Since that time, many advances in retinal imaging have taken place, including fundus photographs taken with the first fundus camera, shown in Fig. 1(b) (Jackman & Webster, 1886), the flash bulb used for retinal illumination, and the scanning laser ophthalmoscope (Webb *et al.*, 1980). However, in spite of
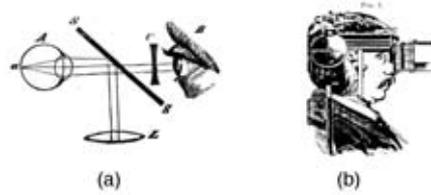
Figure 1.   The direct ophthalmoscope and the fundus camera invented in the 19th century by (a): Hermann von Helmholtz (1851), and (b): Jackman and Webster (1886), respectively.
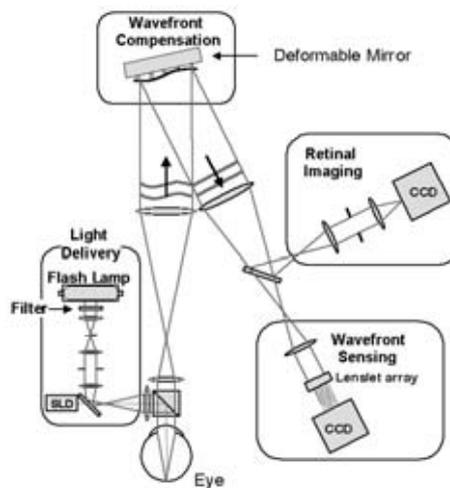

Figure 2.   A schematic diagram of an adaptive optics ophthalmoscope. The wave aberration of the eye is measured with a Hartmann-Shack wavefront sensor. The deformable mirror corrects the aberrations of the eye by altering its shape. After this correction, a flash lamp delivers light to the retina and a high-resolution image of the cone mosaic is recorded by a scientific-grade CCD array.

all the advances in ophthalmoscopy, the quality of the retinal image was always limited by the optics of the eye. In the 150 years since the invention of the ophthalmoscope, compensation for the eye's aberrations has been limited to a correction of only defocus and astigmatism. However, there are myriads of higher order aberrations that are known to degrade retinal image quality in the human eye (Liang & Williams, 1997).

As described in the previous chapter, adaptive optics may be used to correct these higher order aberrations. The schematic principle of an adaptive optics system used to obtain microscopic retinal images is shown in Fig. 2. If the eye were perfect, light that originated from a single point on the retina would form parallel rays, or a plane wave, as it emerged from the pupil. However, in the case of a real eye, aberrations distort the shape of the wavefront. These aberrations can be measured by a wavefront sensor and are corrected by altering the shape

of a deformable mirror that exactly compensates for the eye's wave aberration. For the purposes of retinal imaging, a Krypton flash lamp may then be used to illuminate the retina. The exposure time of a single flash is 4 ms, which reduces motion blur that may result from small eye movements during an exposure. The lamp provides a broadband, white light source which is filtered with a narrow bandwidth interference filter. A scientific grade CCD camera is positioned in a plane conjugate with the retina in a separate arm of the system to acquire a retinal image.

No Adaptive Optics   **With Adaptive Optics**

(a)   10 arc min   (b)   (c)
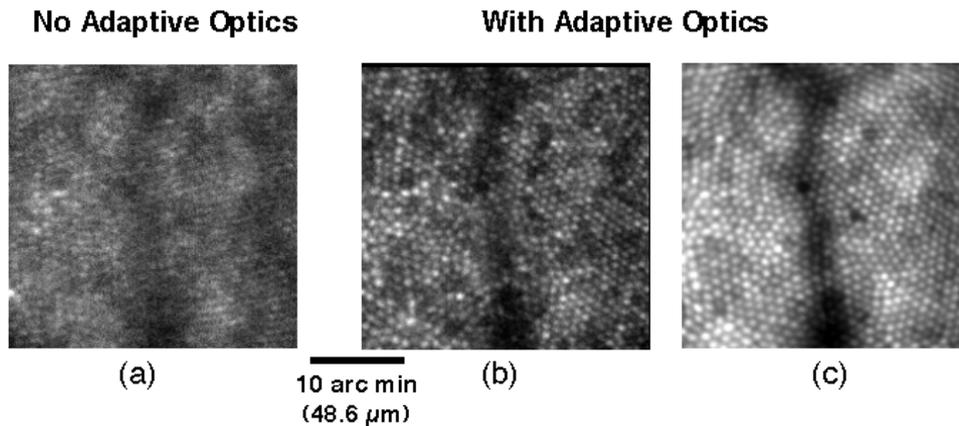   (48.6 µm)

Figure 3.   Images of the same retinal location (a) before and (b) after the use of adaptive optics. Each image was taken one degree nasal to the fovea. (c) shows the registered sum of 61 compensated images of the same patch of retina (Roorda & Williams, 1999).

Fig. 3 shows images of the same retinal location (1 deg from the center of the fovea) for subject JW. The uncompensated image on the left is a single snapshot taken when only defocus and astigmatism were corrected and represents one of the best images of a photoreceptor array obtained without the use of adaptive optics. The middle image shows the improvement in the quality of the retinal image with adaptive optics. After adaptive compensation, the photoreceptor array is better resolved and has higher contrast. While most photoreceptors can be seen in a single corrected image, there are some regions where the reflected light is weak and the signal to noise is too low to detect every cone. Eye movements and safety limits for retinal light exposure preclude simply increasing the signal by increasing exposure times or flash intensity. However, by registering and adding a series of images together, further improvements can be obtained in the quality of retinal images. The rightmost image in Fig. 3 shows the average of 61 frames obtained at the same retinal location in which all frames were registered with cross-correlation techniques. The dark line across the center of each image in Fig. 3 is a shadow cast by an out-of-focus capillary, lying a plane above the photoreceptor layer.

Fig. 4 shows images obtained from a Macaque retina. This image was constructed by registering and adding together a series of 1 degree images. The
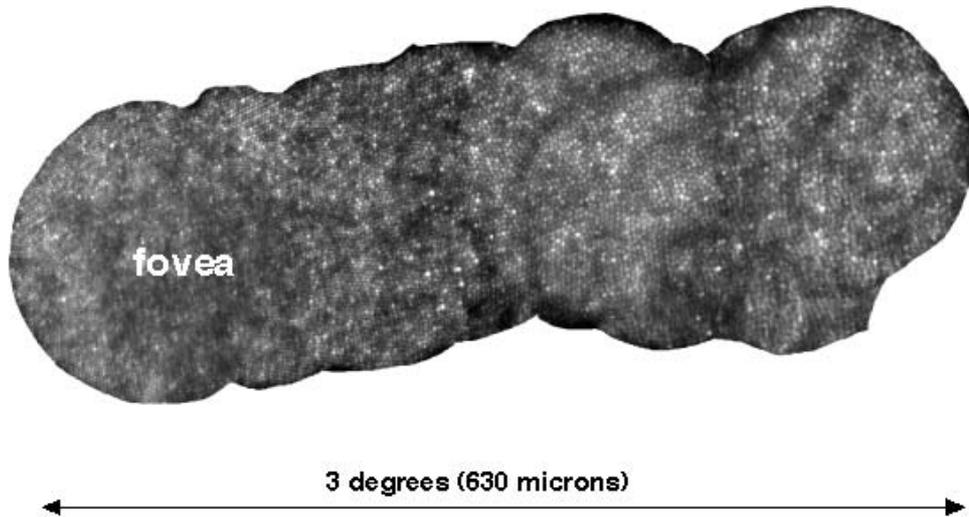
3 degrees (630 microns)

Figure 4.   Photoreceptor mosaic of the Macaque retina. Aberration compensation was obtained one degree nasal to the foveal center, and all images were taken with the same state of compensation.

Macaque's aberrations were compensated at only one retinal location, 1 degree from the center of the fovea, and this compensation was used to capture images from the foveal center to an eccentricity of three degrees. Fig. 4 shows that the aberrations are fairly uniform across this patch of retina, indicating that the isoplanatic patch size is at least as large as this composite image. In addition, one can clearly see that the cones are smallest and most tightly packed at the center of the fovea and become larger and less dense with increasing eccentricity.

3.   Application of Adaptive Optics for Basic Science

Before the advent of adaptive optics for the human eye, studies of the retina on a spatial scale of single cells have required physically removing the retina from the back of the eye, causing irreversible changes in retinal tissue. In addition, once the biological properties of the excised retinal structures are measured, there is no longer a direct way to correlate these characteristics with visual performance or perception. Adaptive optics is a very powerful tool because it is a non-invasive imaging method that can photograph microscopic features in the living retina while leaving the retina intact and unaffected to perform subsequent measurements of visual perception and performance.

It has been known for some time that photoreceptors behave like optical waveguides (Stiles & Crawford, 1933), but it has not been possible to measure the fiber-like properties of single primate photoreceptors in their undisturbed state within the living eye. The ability to image living photoreceptors with adaptive

optics offers the possibility to improve our understanding of the light-collecting properties of the retina.

Until recently, the spatial arrangement and relative numbers of the three cone classes were not well-characterized in the human retina, though we have known that color vision is mediated by three classes of cones for nearly 200 years. Combining high resolution imaging through adaptive optics with retinal densitometry of the cone photopigments, Roorda and Williams have successfully identified all three cone classes in the living human eye (Roorda & Williams, 1999). In this section, these two examples will be described.

3.1. Waveguide properties of photoreceptors

Light entering the retina goes through several layers before being absorbed by photopigments in each photoreceptor. A majority of the retina is transparent to visible light and most light paths are not seriously altered when propagating to the photoreceptors. The photoreceptors, however, actually behave like optical waveguides, and are angularly tuned to selectively collect incident light and funnel it through the photosensitive pigments. The optical waveguide structure of the cone photoreceptors gives rise to their angular tuning properties. This

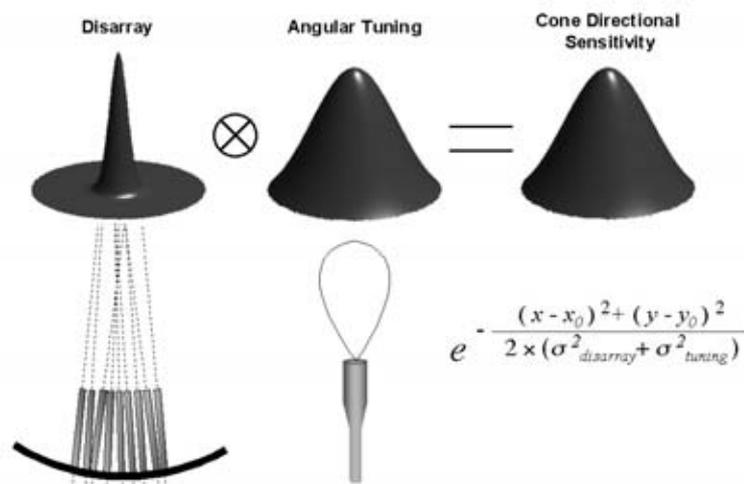$$e^{-\frac{(x-x_0)^2 + (y-y_0)^2}{2 \times (\sigma^2_{disarray} + \sigma^2_{tuning})}}$$

Figure 5.   Schematic description of the cone's directional sensitivity. As shown in the figure, cone directional sensitivity is obtained by convolving the disarray of cones with their angular tuning.

property was first detected when Stiles and Crawford measured the light sensitivity of the eye as a function of illumination angle, altering the incident angle of the light by incrementally translating a small artificial pupil across the optics of the eye. The overall directional sensitivity of an ensemble of cones is the result of a convolution of the disarray of the ensemble of cones in the retina with the angular tuning functions of the individual cones. This concept is illustrated in Fig. 5.

Some psychophysical and objective studies have indirectly attempted to unveil this property of the photoreceptors (MacLeod, 1974; Burns *et al.*, 1995) and have

agreed that the spread of the cone disarray is small relative to the tuning function of the cones. However, no direct measurements of the waveguide properties of the cones have ever been done in living human eyes.
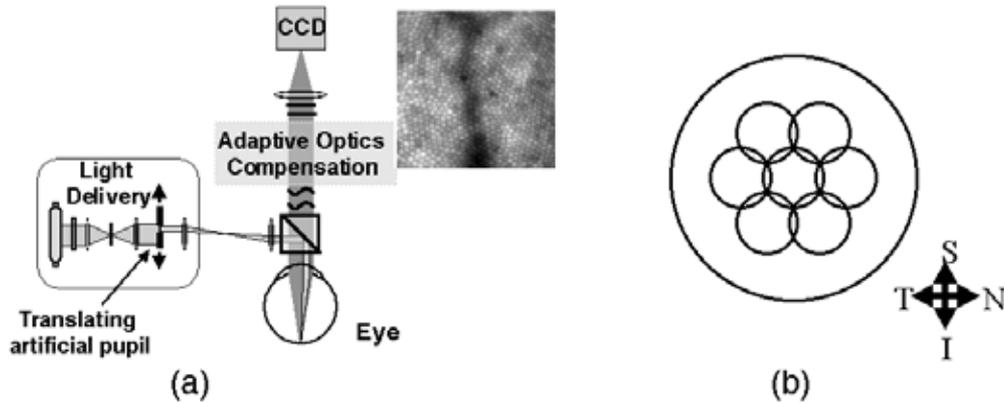

Figure 6.   (a) Schematic configuration of the cone directional sensitivity experiment (Roorda & Williams, 2000). Changes in the illumination angle of the incident light were achieved by translating the position of an artificial pupil placed in a plane conjugate with the eye's pupil. (b). Seven entrance beam locations were tested.

We can use adaptive optics ophthalmoscopy to further investigate and more directly solve this problem, as adaptive optics allows for the imaging of single cone photoreceptors and the direct measurement of the optical properties of individual cones in the living human eye. Here we discuss a preliminary experiment used to measure the cone's angular tuning properties (Roorda & Williams, 2000), shown in Fig. 6. The tuning properties of the cone can be determined by measuring the amount of light that gets coupled into each cone as a function of illumination angle. If a cone is obliquely illuminated with respect to its optical axis, less light will be coupled into a cone and therefore, less light will be reflected from that cone. In this experiment, the angle of illumination was changed by translating a small artificial pupil relative to the eye's natural pupil. The artificial pupil placed in the illumination path was conjugate with the eye's pupil, as shown in Fig. 6(a).

The same exit pupil was always used for imaging, so the light acceptance angles of the cones, rather than the directional reflectivity of the cone array, were measured. Seven different entrance pupil locations in a hexagonal pattern were adopted within the eye's pupil and are shown in Fig. 6(b). For each illumination angle, several images of the same patch of retina were collected in order to obtain enough signal to detect the differences in reflectivity of the cone mosaic.

The images obtained at each illumination angle for subject JP are shown in Fig. 7. For this subject, the center of the illumination angle was adjusted to be the best estimate of his Stiles-Crawford peak, where the amount of the reflected light came to its maximum. Each of the seven images is a registered sum of ten individual images. As the illumination angle moves away from the
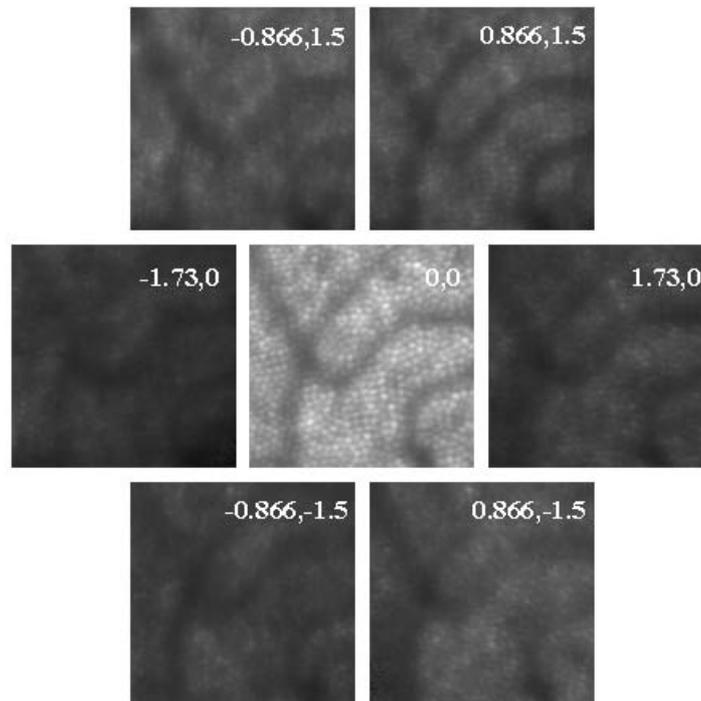
Figure 7.   Retinal images taken at each entrance beam location after compensating for the wave aberration of the eye. Each image is the registered sum of 10 images of the same retinal location. The numbers in the upper-right hand corner of each image correspond to the displacement of the artificial pupil (in mm) in the horizontal and vertical directions. (A location of (0,0) indicates that the artificial pupil was exactly centered on the subject's Stiles-Crawford peak.)

center of the pupil, the amount of light reflected from the retina varies and the contrast in the image decreases. However, the resolution of each registered image was approximately the same since the wave aberration was corrected by the deformable mirror before acquiring each image. The only change between the center and surrounding images is the reflectivity of the sample. Some contrast reduction in the surrounding images is observed because light that leaks from the cones contributes to the overall background light in the image. The same trend was observed in a second subject. Even though the full analysis of the tuning of individual cones is not yet complete, this result shows the dramatic changes in reflectivity that occur by changing the incident illumination angle and offers the opportunity to measure the waveguide properties of each individual cone in the image.

3.2. The trichromatic photoreceptor mosaic

In 1802, Young stated definitively that human color vision depends on three fundamental channels. For many years psychophysical observations have successfully attempted to characterize the spectral properties of these channels without much success in determining the relative density, packing geometry and location of the three cone classes in the normal human retina. The most thoroughly studied and well-understood class of cones has been the S-cones. However, the L- and M- cone mosaics have proven to be much more difficult to distinguish. No morphological differences distinguish the L- and M-cones, and the similarity in the absorption spectra of their photopigments made it extremely difficult to selectively label them. Some techniques that have been successful in providing topographic information have relied on differences in the absorption spectrum of the M- and L- cone photopigments. Other approaches, such as psychophysical experiments and mRNA analysis (Gowdy & Cicerone, 1998; Hagstrom *et al.*, 1998) have also been conducted to classify the arrangement of human M- and L-cones or the ratio of L- and M- cones across the human retina. In this section, we describe a method used in conjunction with adaptive optics to obtain the first images of the arrangement of S-, M-, and L- cones in the living human eye, as reported by Roorda and Williams (Roorda & Williams, 1999). For those interested in further details not presented below, we refer the interested reader to Williams and Roorda (Williams & Roorda, 2000).
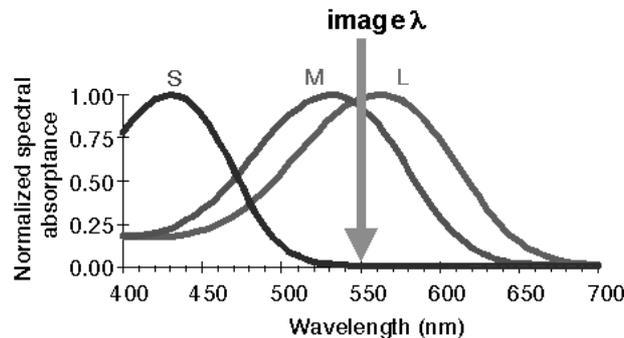

Figure 8.   The relative sensitivity of L-, M-, and S- cones.

When the retina is exposed to an intense light source and the photopigment inside each photoreceptor has absorbed its maximal amount of light, the photoreceptor array is said to be in a fully bleached condition. Fully bleached conditions are obtained by exposing the eye to a bright light prior to taking an image. The photoreceptor can no longer absorb light until the photopigment has had ample time to regenerate, usually on the order of five minutes. Once the photopigment has been fully restored, the respective photoreceptors are again ready to absorb light and are in a dark-adapted condition. In the dark adapted state, the pigment within the cones absorbs the light and less light is reflected from the retina, rendering a lower contrast image of the mosaic. We can therefore

classify individual cones by taking and comparing images of the photoreceptor mosaic when the photopigment was fully bleached to those when the photopigment was dark-adapted or selectively bleached by a light specifically tuned to the absorption spectrum of an individual cone class. The spectral sensitivities of the three cone classes are shown in Fig. 8. As shown in the figure, the light used in this experiment to image the retina has a wavelength of 550 nm and is strongly absorbed by both the M- and L-cones while leaving the S-cones primarily unaffected. Only the cones with absorption spectra at 550 nm will absorb the light, appearing dim in an image of the mosaic, while the S-cones still contain all of their photopigment and appear bright. Fig. 9(a) shows an image obtained
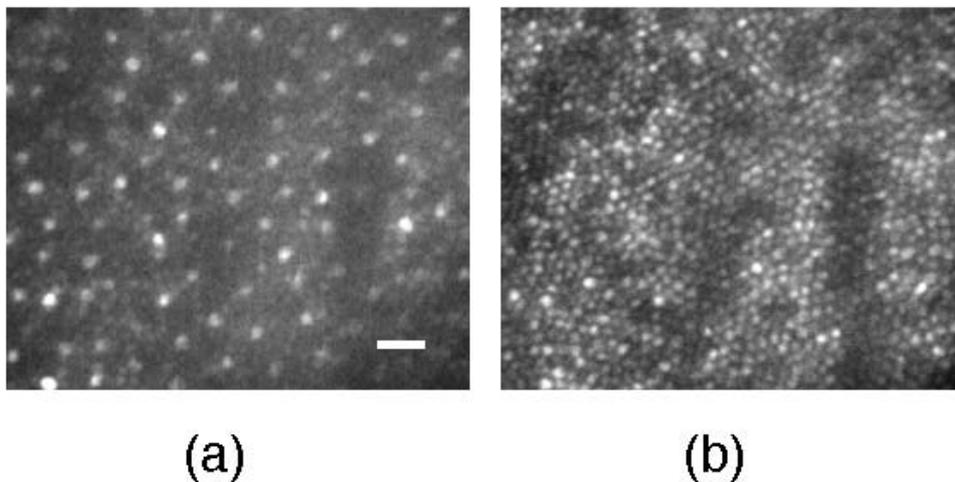

(a)   (b)

Figure 9.   Retinal images taken in the (a): dark adapted condition, and the (b): fully bleached condition. Scale bar indicates 5 minutes of arc.

after dark adaptation, while Fig. 9(b) is an image obtained after the mosaic was fully bleached. In the image of the dark adapted retina, a sparse array of highly transmitting cones can be observed and are presumably the S-cones. As a result, it now becomes possible to distinguish S-cones from the M- and L-cones this dark adapted image with the fully bleached image. The absorptance of each cone is calculated by subtracting the ratio of the absorptance of a dark adapted image to that of a fully bleached image from one. S-cones will then appear as a sparse array of dark cones in the resulting absorptance image.

To distinguish L-cones from M-cones, we took images immediately following either of two bleaching conditions, illustrated in Fig. 10. In the first bleaching condition, shown in Fig. 10(a), a dark adapted retina was exposed to a 650 nm light that selectively bleached the L-cone pigment. An image taken after a 650 nm bleach will show only the M-cones absorbing light. The absorptance image for the 650 nm bleach revealed dark, low-absorptance L-cones that have been heavily bleached and bright, highly absorbing M-cones spared from bleaching. In the second condition, a 470 nm light selectively bleached the M-cone pigment as shown in Fig. 10(b). The absorptance images for the 470 nm bleach show
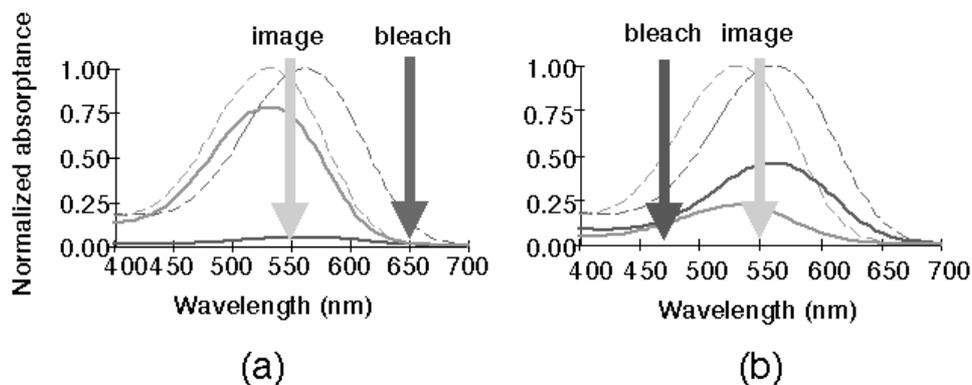
Figure 10.   Method of selective bleaching. The normal absorptance spectra for the M- and L-cones before bleaching are shown with the gray and black dashed lines, respectively. (a): A 650-nm bleaching light is used to selectively bleach away the L-cone pigment (the resulting spectrum for which is shown in solid black) sparing the M-cone pigment (the spectrum shown in solid gray). (b) A 470-nm bleaching light is used to selectively bleach the M-cone pigment prior to taking an image.

selective bleaching of M-cones but the effect is reduced due to the similarity in the M- and L-cone sensitivities at this wavelength. Although the bleach is less selective due to the nature of the spectral pigments, the bleach leaves the L-cones with a greater absorptance. Bleaching levels had to be carefully set to maximize the difference in concentration between the L- and M-cone classes since too much bleaching at any wavelength would leave no concentration of pigment in either cone class. Fig. 11 shows scatter plots of absorptances for subject JW. Each point in the scatterplot indicates the absorptances of a single cone following a 470 and 650 nm bleach. The vertical axis shows the absorptance after a 650 nm bleach and the horizontal axis is the absorptance of the same cone after a 470 nm bleach. The S-cones have already been removed from the set of cones displayed in the figure. The L-cones most likely make up the lower distribution since, after a 640 nm bleach, the L-cones should appear relatively less absorbent than the M-cones. For this subject, the cloud of points produces a bimodal distribution. The bimodality can be seen more easily in the corresponding histogram, which is shown in Fig. 12. Angle θ is defined on the scatter plot in Fig. 11 and the histogram of the number of cones as a function of that angle is plotted in Fig. 12. The mode on the left would represent the L-cones and the mode on the right represents the M-cones. If these modes represent L- and M-cones, then only a single mode should be observed in a similar experiment on a subject who lacks one cone class. This prediction was confirmed by data obtained from a protanope who lacks L-cone pigment.

Ignoring the S-cones, we fit the histogram to a double Gaussian. The overlap of these Gaussians provided an estimate of the fraction of cones that were misidentified. To estimate the relative number of L- and M-cones, we assigned all cones
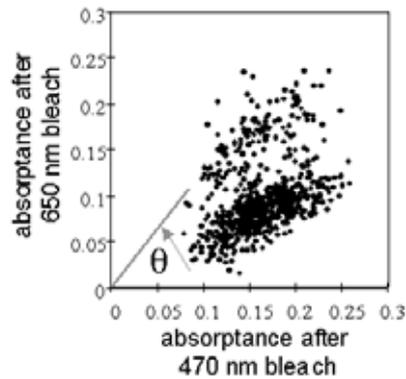
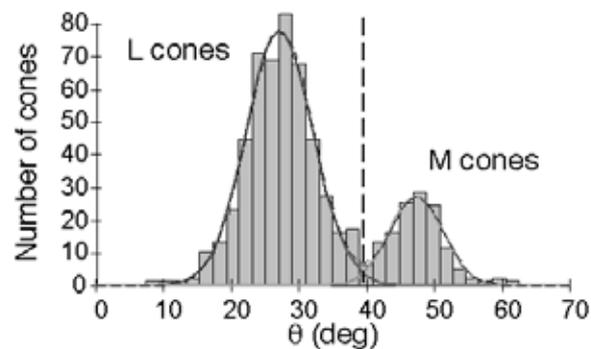Figure 11.   Scatter plots of individual cone absorptances for a subject JW.

Figure 12.   Histogram of the scatter plot as a function of angle θ which was defined in Fig. 11. The two solid lines show the best-fit Gaussian curves for each distribution.

to the left of the cross-over of the two Gaussians as L-cones and the ones to the right as M-cones. The relative number of L- and M-cones has been measured on two color normal subjects, whose images are shown in Fig. 13. Fig. 13(a) is obtained from subject JW, and 13(b) from subject AN. Some of the cones beneath the capillary were not analyzed due to the fact that they were not visible in all images. The relative number of L- and M-cones differs greatly between these two subjects. In two separate patches of retina, one from the nasal and one from the temporal fovea, subject JW had a mean L-to M-cone ratio of 3.79 while AN had a ratio of 1.15. Although they have a large difference in their relative cone ratios, both are classified as being color normal by several vision tests. Those further interested in the visual characteristics and perception of these two subjects are referred to Brainard *et al.*(2000).

Figure 13.   Pseudocolor images of the trichromatic cone mosaic (Roorda & Williams, 1999). Blue, green, and red circles represent the S-, M-, and L-cones, respectively for (a) subject JW, and (b) subject AN. The scale bar represents 5 minutes of arc.

4.   Clinical Applications of Adaptive Optics

In addition to the basic science described above, it is possible to use adaptive optics in the clinic. Adaptive optics may provide earlier detection, better diagnosis, and more effective treatment of retinal disease. For example, the ability to resolve photoreceptors in the living eye could increase our understanding of cone distrophies. Glaucoma, a disease in which blindness ensues from the gradual loss of optic nerve fibers, can only be detected with conventional imaging techniques after a significant amount of damage has already taken place. More accurate measurements of the nerve fiber layer thickness around the optic nerve head will allow earlier detection of this disease. Another example is age-related macular degeneration (AMD), which causes a progressive loss in the central vision of 10% of the population over age 60.
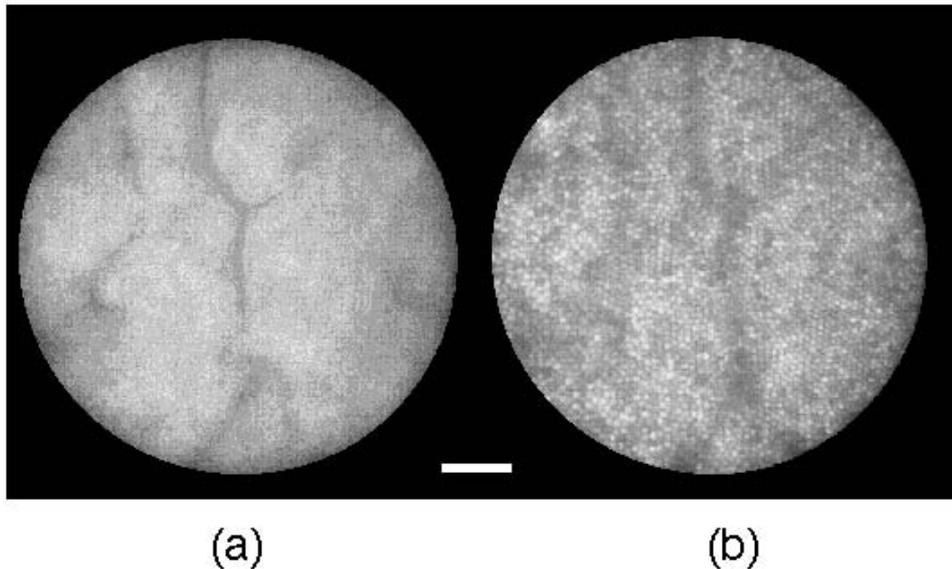

(a)   (b)

Figure 14.   (a) Image taken by focusing on a layer containing capillaries in the living retina. (b) By focusing approximately 100 μm deeper in the retina, the photoreceptors come into focus. The capillaries now appear as kim, out-of-focus shadows on the photoreceptor mosaic. Scale bar indicates 10 minutes of arc.

It has been suggested that there may be a subclinical loss of receptors associated with AMD that is not detectable in the fundus by current imaging methods. Adaptive optics could reveal the early stages of the development and progression of this disease. In one form of AMD, deterioration of the retina begins with a formation of new blood vessels in the choroid and an eventual leakage of fluid beneath the retina around the fovea. This can eventually cause blindness in the most highly resolving location in the visual field. Another disease that effects the retina, diabetes, causes the formation of new, often leaky, blood vessels, and microaneurysms in the retinal vasculature. Treatment for both diseases requires accurate delivery of a photocoagulating laser beam, which could benefit from a higher resolution view of this critical retinal region. Adaptive optics can be used to image the smallest blood vessels in the retina without the use of invasive dyes such as those used in fluorescein and indocyanine green angiography, and offers the potential for earlier detection and laser treatment with greater precision. An image of the capillaries at the edge of the avascular zone is shown in Fig. 14 (a). Moreover, in combination with improved eye-tracking technology, adaptive optics may make it possible to deliver with improved accuracy a more compact and less invasive photocoagulating beam.
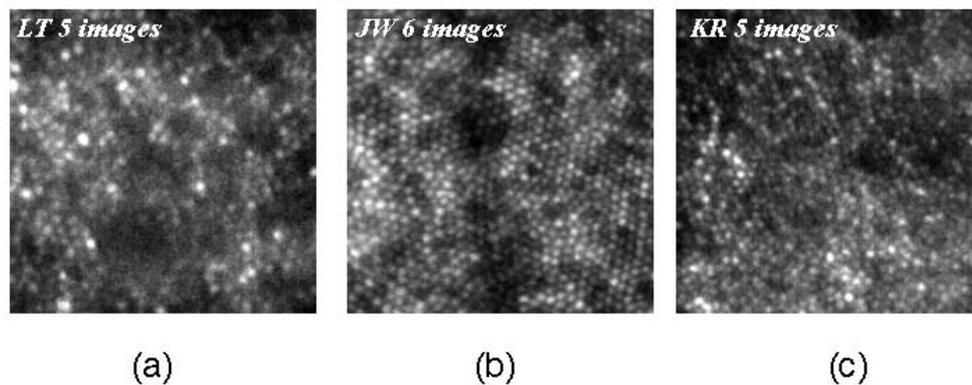

Figure 15. Retinal images taken from (a) a patient with cone dystrophy, and (b, c) healthy subjects. While an entire array of cones can be seen for the healthy subjects, large patches of retina with no visible cones are seen for those of the pathological patient in (a).

The ability to image microscopic structures in living retina may be particularly valuable for tracking retinal processes that vary over time at a microscopic spatial scale, such as the progression of retinal disease or the development of the normal retina. Current methods using excised retina require piecing together evidence from large numbers of retinas, while microscopic imaging of the living retina could reveal the whole temporal sequence in individual eyes. For example, in retinitis pigmentosa, mutated genes that are responsible for the production of rhodopsin lead to the death of rod photoreceptors and ultimately results in blindness. The evaluation of therapies for this disorder could be aided by higher

resolution retinal imaging that would allow the integrity of individual receptors to be tracked over time.

Fig. 15(a) shows an image obtained from a patient who has cone dystrophy. For comparison, Fig. 15(b) and (c) are images obtained from healthy subjects. While we can see a contiguous array of cones in the healthy eyes, the patient with cone dystrophy has large patches of retina with no visible cones. This image demonstrates the possibility of using adaptive optics in verifying the diagnosis by looking directly at the high-resolution images.

One of the biggest advantages of adaptive optics is that we can obtain a precise, high-resolution images of the retina. Adaptive optics can be used to not only to monitor any microsurgery, but can also test the efficacy of the treatment method.

5. Summary and Further Improvement

In this chapter, we described several applications of adaptive optics, not only for basic vision science, but also for clinical areas. Adaptive optics is a very strong and useful tool that will continue to explore and create new frontiers in vision science.

Digital imaging offers the possibility to post-process images, improving image quality and allowing for the extraction of even more information about the retina from these images. Phase diversity (Gonsalves, 1982; Paxman & Fienup, 1988) offers a promising method to improve fundus images while simultaneously estimating the eye's aberrations. This improvement could further expand the use of adaptive optics in clinical and low-cost applications.

References

Brainard, D. H., Roorda, A., Yamauchi, Y., Calderone, J. B., Metha, A., Neitz, M, Neitz, J., Williams, D. R. & Jacobs, G. H., 2000, J. Opt. Soc. Am. A, 17, 607.

Burns, S. A., Wu, S., Delori, F. C. & Elsner, A. E., 1995, J. Opt. Soc. Am. A, 12, 2329.

Gonsalves, R. A., 1982, Opt. Eng. 21, 829.

Gowdy, P. & Cicerone, C. M., 1998, Vision Res., 38, 2575.

Hagstrom, S. A., Neitz, J. & Neitz, M., 1998, NeuroReport, 9, 1963.

Jackman, W. T. & Webster, J. D., 1886,The Philadelphia Photographer, 23, 340.

Liang, J. & Williams, D. R., 1997, J. Opt. Soc. Am. A, 14, 2873.

MacLeod, D. I. A., 1974, Vision Res., 14, 369.

Paxman, R. G. & Fienup, J. R., 1988, J. Opt. Soc. Am. A, 5, 914.

Roorda, A. & Williams, D. R., 1999, Nature 397, 520.

Roorda, A. & Williams, D. R., 2000, Invest. Ophthal. Vis. Sci., 41, S100.

Stiles, W. S. & Crawford, B. H., 1933, Proc. R. Soc. Lond. B, 112, 428.

Webb, R. H., Hughes, G. W. & Pomerantzeff, O., 1980, Appl. Opt., 19, 2991.

Williams, D. R. & Roorda, A., 2000, in Color Vision, From genes to perception, ed. Gegenfurtner, K. R., & Sharpe, L. T.(Cambridge University Press), 113.